A NANOSCALE MESHFREE PARTICLE METHOD WITH THE IMPLEMENTATION OF THE QUASICONTINUUM METHOD

SHAOPING XIAO

Department of Mechanical and Industrial Engineering and Center for Computer-Aided Design,
The University of Iowa, 3131 Seamans Center, Iowa City, Iowa 52242, USA
shaoping-xiao@uiowa.edu
http://www.engineering.uiowa.edu/~sxiao

WEIXUAN YANG

Department of Mechanical and Industrial Engineering and Center for Computer-Aided Design,
The University of Iowa, 116 Engineering Research Facility, Iowa City, Iowa 52242, USA
weixuan-yang@uiowa.edu

Since meshfree particle methods have advantages on simulating the problems involving extremely large deformations, fractures etc., they become attractive options to be used in the hierarchical multiscale modeling to approximate a large number of atoms. We propose a nanoscale meshfree particle method with the implementation of the quasicontinuum technique in this paper. The intrinsic properties of the material associated with each particle will be sought from the atomic level via the Cauchy-Born rule. The studies of a nano beam and a nano plate with a central crack show that such a hierarchical modeling can be beneficial from the advantages of meshfree particle methods.

Keywords: meshfree particle method; nanoscale; quasicontinuum; crack.

1. Introduction

Numerical simulation has become a powerful tool and has made a significant contribution to the fields of nano science and technology. The efficient numerical methods will stimulate the nanotechnology development, such as the nanoscale material and device design. The popularly used molecular dynamics was expected to be one of the candidates. However, researchers have found that the molecular dynamics simulation has limitations on both length and time scales. Recently, multiscale methods have been of interest in the field of computational nano mechanics and materials science because they can perform the simulation for large nano systems.

There are two types of multiscale methods: concurrent multiscale methods and hierarchical multiscale methods. The concurrent multiscale methods treat different length scales simultaneously by using different numerical methods. The recently developed concurrent multiscale techniques mainly focused on the coupling methods between the continuum and molecular models. Abraham and his coworkers [Abraham et al. 1998; Broughton et al. 1999] developed a methodology called MAAD (Macro-Atomistic-Ab initio-Dynamics), which couples a tight-binding quantum mechanical calculation,

molecular dynamics, and a finite element method. Rudd and Broughton [Rudd and Broughton 1998; Rudd 2001] proposed a coarse-grained method. They superimposed the atomistic Hamiltonian on a continuum Hamiltonian so a coarse scale domain was used to represent the fine scale domain. Wagner and Liu [Wagner and Liu 2003] have proposed a bridging scale method in which the molecular displacements were decomposed into a molecular scale and a continuum scale. Belytschko and Xiao [Belytschko and Xiao 2003; Xiao and Belytschko 2004] developed a bridging domain coupling method by overlapping the continuum model and the molecular model via the bridging domain. Their method can efficiently eliminate the nonphysical wave reflection that usually occurs at the interface of different length scales.

Hierarchical multiscale methods use the continuum approximation to model a large group of molecules. The continuum approximation is based on the properties of the atomic model, such as an MD model. One can use a homogenization procedure, like the Cauchy-Born rule [Tadmor et al. 1996; 2000], in the continuum model. Therefore, the intrinsic properties of the material at the atomic level can be obtained and embedded in the continuum model. The classical Cauchy-Born rule states that the deformation is locally homogeneous, and this model is also called the quasicontinuum model. Based on an extended version of the local quasicontinuum model [Smith et al. 2001], Smith and his coworkers reported that the simulations of silicon nanoindentation were capable of handling complex crystal structures. Diestler et al. [Diestler et al. 2002; Wu et al. 2003] developed an alternative "static" finite-element coarse-graining description which is an extension to nonzero temperatures of the quasicontinuum procedure. The major drawbacks of hierarchical multiscale methods relate to the difficulties in modeling defects in molecular lattices, dislocations, crack initiation and growth, as well as limitations arising from the homogeneous deformation model used. There are several algorithms to solve these issues. Rodney and Phillips [Rodney and Phillips 1999] built quasicontinuum simulations of dislocations lying in intersecting slip planes, and calculated the threshold stress required to break the dislocation junction. Mortensen and his coworkers [Mortensen et al. 2002] used a mixed local/nonlocal quasicontinuum with some modifications to study a cross-slip of screw dislocations and job mobility in copper. With the wide usage of the Cauchy-Born rule, Arroyo and Belytschko [Arroyo and Belytschko 2002; 2003] found that the classical Cauchy-Born rule has some difficulties for many important situations, such as in single-layer curved crystalline sheets. They developed a methodology called the exponential Cauchy-Born rule to solve this issue.

Finite element methods are often used for modeling continua in multiscale methods based on the quasicontinuum approach. However, meshfree particle methods are more attractive for usage in a variety of situations, including problems with moving boundaries, discontinuities, and extremely large deformations. In general, the meshfree particle methods include field approximation based methods [Belytschko et al. 1994] or kernel approximation based methods [Randles and Libersky 1996]. Belytschko et al. [Belytschko et al. 2000; Belytschko and Xiao 2002; Xiao and Belytschko 2005] found that the kernel based meshfree particle methods had two instability properties: an instability due to rank deficiency and a tensile instability. Nodal integration [Beissel and Belytschko 1996] may result in one of the instabilities due to rank deficiency for some problems. Stress point integration scheme [Dyka et al. 1997] can stabilize this instability. The tensile instability is also called the distortion of material instability [Xiao and Belytscko 2005]. When using meshfree particle methods with the stress point integration

scheme, the Lagrangian kernel, which is a function of the material coordinates, exactly reproduces the material instability of the constitutive equation, while the Eulerian kernel, which is a function of the spatial coordinates, extremely distorts the material instability. Therefore, the meshfree particle method, with a Lagrangian kernel and the stress point integration scheme, will provide a stable and efficient method [Rabczuk et al. 2004]. In this paper, we will implement the quasicontinuum technique into the meshfree particle method with a Lagrangian kernel. Such a nanoscale meshfree particle method will be used to simulate nano systems containing a large number of atoms.

The outline of this paper is as follows: A meshfree particle method with a Lagrangian kernel is introduced in Section 2. In Section 3 the implementation of the quasicontinuum technique into the meshfree particle method is described. Several examples are studied in Section 4. The numerical results will be compared with the results of atomistic simulations. The conclusions and discussions follow.

2. Meshfree Particle Methods

2.1. *Governing equations*

One of the physical principles governing the continuum is the conservation of momentum. It can be written as the following equation under a so-called total Lagrangian description in the reference configuration Ω_0,

$$\frac{\partial P_{ji}}{\partial X_j} + \rho_0 b_i = \rho_0 \ddot{u}_i \tag{1}$$

where ρ_0 is the initial density, $\mathbf{P}$ is the first Piola-Kirchhoff stress tensor, $\mathbf{X}$ are the material (Lagrangian) coordinates, $\mathbf{b}$ is the body force per unit mass, $\mathbf{u}$ is the displacement and the superposed dots denote material time derivatives. Eq. (1) can be written as the spatial form of the momentum equations under the Eulerian description in the current configuration Ω,

$$\frac{\partial \sigma_{ji}}{\partial x_j} + \rho b_i = \rho \ddot{u}_i \tag{2}$$

where ρ is the current density, $\boldsymbol{\sigma}$ is the Cauchy stress tensor, and $\mathbf{x}$ are the spatial (Eulerian) coordinates. By conservation of mass,

$$\rho J = \rho_0 \tag{3}$$

where J is the Jacobian determinant of deformation gradient $\mathbf{F}$, and it is defined by

$$J = \det(\mathbf{F}), \qquad F_{ij} = \frac{\partial x_i}{\partial X_j} \tag{4}$$

It can be seen that the two above forms of momentum equations in Eq. (1) and Eq. (2) are identical and differ in form only because they are expressed in different descriptions [Belytschko et al. 2001]. In this paper, we use the Lagrangian description. The Galerkin weak form of the momentum conservation equation is

$$\int_{\Omega_0} \delta u_i \rho_0 \ddot{u}_i d\Omega_0 = \int_{\Omega_0} \delta u_i \rho_0 b_i d\Omega_0 - \int_{\Omega_0} \delta F_{ij} P_{ji} d\Omega_0 + \int_{\Gamma_0} \delta u_i \bar{t}_i d\Gamma_0 \tag{5}$$

where δu_i is the test function, and $\bar{t}_i$ is the prescribed boundary traction. The discrete equations of motion can be derived from weak form, Eq. (5), for dynamic problems.

2.2. *Particle method approximations and kernel functions*

In particle methods, displacements can be approximated by

$$\mathbf{u}^h(\mathbf{X},t) = \sum_I w_I(\mathbf{X})\mathbf{u}_I(t) \tag{6}$$

where $w_I(\mathbf{X})$ are called Lagrangian kernel functions [Belytschko and Xiao 2002] because they are functions of the material (Lagrangian) coordinates. If the spatial (Eulerian) coordinates are used, the approximation of displacements can be written in terms of the Eulerian kernel functions as follows:

$$\mathbf{u}^h(\mathbf{x}(t),t) = \sum_I w_I(\mathbf{x}(t))\mathbf{u}_I(t) \tag{7}$$

In this paper, we use the Lagrangian kernel functions because meshfree particle methods with a Lagrangian kernel function are more stable than the ones with an Eulerian kernel function [Belytschko and Xiao 2002]. The Lagrangian kernel functions can be obtained from the weight function $W(r)$ as

$$w_I(\mathbf{X}) = w(\mathbf{X} - \mathbf{X}_I) = \frac{W(\mathbf{X} - \mathbf{X}_I)}{\sum W(\mathbf{X} - \mathbf{X}_I)} \tag{8}$$

which is the moving least square approximation that reproduces constant functions. In this paper, we use a quartic spline weight function,

$$W(s) = \begin{cases} 1 - 6s^2 + 8s^3 - 3s^4 & for \quad s \le 1 \\ 0 & for \quad s > 1 \end{cases} \tag{9}$$

where $s = r/h$, $r = \|\mathbf{X} - \mathbf{X}_I\|$, and h is a measure of the size of the support, which is determined by a dilation parameter D_{mx}. We define $h = D_{mx}\Delta X$ for uniformly spaced particles in one dimension. The kernel functions are of compact support, i.e., $w_I(\mathbf{X}) > 0$ only in the neighborhood of $\mathbf{X}$.

We can see that, from Eq. (8), the kernel functions, $w_I(\mathbf{X})$, obviously reproduce the constant functions, i.e. $\sum_I w_I(\mathbf{X}) = 1$, but not the linear functions. In other words, one can find that $\sum_I \frac{\partial w_I(\mathbf{X})}{\partial X_i} X_{Ij} \ne \delta_{ij}$. Krongauz and Belytschko [Belytschko et al. 1998] developed a correction that enables the derivatives of the constant or linear functions to be reproduced exactly. The corrected derivatives of displacements are denoted by $L_{ji}(\mathbf{X},t)$ and are approximated by

$$L_{ji}(\mathbf{X},t) = \sum_I G_{iI}(\mathbf{X})u_{jI}(t) \tag{10}$$

where $G_{iI}(\mathbf{X})$ are the corrected derivatives of the Lagrangian kernel functions. Note here that $L_{ji}(\mathbf{X},t)$ is different from $\partial u_j^h(\mathbf{X},t) / \partial X_i$ with u_j^h defined by Eq. (6). The corrected derivatives are defined as linear combinations of the exact derivatives of the kernel

functions so the linear functions (coordinates for instance) can be reproduced by the meshfree particle approximation,

$$\sum_I G_{iI}(\mathbf{X})X_{Ij} = \sum_I a_{ik}\frac{\partial w_I(\mathbf{X})}{\partial X_k}X_{Ij} = \delta_{ij} \tag{11}$$

The above can be written in a matrix form,

$$\mathbf{A}\mathbf{a}^T = \mathbf{I} \tag{12}$$

where $\mathbf{I}$ is the identity matrix for a three-dimensional approximation,

$$\mathbf{A} = \begin{bmatrix} w_{I,X}X_I & w_{I,Y}X_I & w_{I,Z}X_I \\ w_{I,X}Y_I & w_{I,Y}Y_I & w_{I,Z}Y_I \\ w_{I,X}Z_I & w_{I,Y}Z_I & w_{I,Z}Z_I \end{bmatrix} \tag{13}$$

$$\mathbf{a} = \begin{bmatrix} a_{XX} & a_{XY} & a_{XZ} \\ a_{YX} & a_{YY} & a_{YZ} \\ a_{ZX} & a_{ZY} & a_{ZZ} \end{bmatrix} \tag{14}$$

By solving Eq. (12) for the coefficient matrix $\mathbf{a}$, one can obtain the corrected derivatives of kernel functions, $G_{iI}(\mathbf{X})$. Therefore, the approximation for the derivatives of displacements in Eq. (10) can be written as follows:

$$L_{ji}(\mathbf{X},t) = \sum_I \left[\sum_k a_{ik}(\mathbf{X})w_{I,k}(\mathbf{X}) \right] u_{jI}(t) \tag{15}$$

Then, the gradient of deformation is expressed as

$$F_{ij} = \frac{\partial u_i}{\partial X_j} + \delta_{ij} = L_{ij} + \delta_{ij} \tag{16}$$

2.3. Discrete equations

Substituting Eq. (6), the approximation of displacements, and a similar expansion for $\delta\mathbf{u}(\mathbf{X})$ into the weak form of Eq. (5), the following discrete equations of motion are obtained:

$$m_I \ddot{u}_{iI} = F_{iI}^{ext} - F_{iI}^{int}, \qquad\qquad m_I = \rho_0 V_I^0 \tag{17}$$

where V_I^0 is the volume associated with the particle I, F_{iI}^{ext} and F_{iI}^{int} are the external and internal nodal forces respectively, given by

$$F_{iI}^{ext} = \int_{\Omega_0} \rho_0 w_I b_i d\Omega_0 + \int_{\Gamma_0^t} N_I \bar{t}_i d\Gamma_0 \tag{18}$$

$$F_{iI}^{int} = \int_{\Omega_0} \frac{\partial w_I(\mathbf{X})}{\partial X_j} P_{ji} d\Omega_0 \tag{19}$$

Stationary principles can be applied for conservative, static problems. The equilibrium solutions can be found by searching a set of displacements from which the minimum potential can be obtained, i.e.

$$\begin{aligned} 0 = \delta W(\mathbf{u}) &= \delta W^{int}(\mathbf{u}) - \delta W^{ext}(\mathbf{u}) \\ &= \int_{\Omega_0} \delta F_{ij} P_{ji} d\Omega_0 - \int_{\Omega_0} \delta u_i \rho_0 b_i d\Omega_0 - \int_{\Gamma_0} \delta u_i \bar{t}_i d\Gamma_0 \end{aligned} \tag{20}$$

Note here that Eq. (20) is identical to Eq. (5) if the accelerations are set to equal zero in Eq. (5) for static problems. We can obtain the residual as

$$0 = r_{iI} = \frac{\partial W}{\partial u_{iI}} = \frac{\partial W^{\text{int}}}{\partial u_{iI}} - \frac{\partial W^{\text{ext}}}{\partial u_{iI}} = F_{iI}^{\text{int}} - F_{iI}^{ext} \tag{21}$$

where internal and external nodal forces are defined as Eq. (18) and Eq. (19).

The increments of the internal and external forces can be related to the increments of nodal displacements by stiffness matrices via the Newton method:

$$\Delta \mathbf{F}^{\text{int}} = \mathbf{K}^{\text{int}} \Delta \mathbf{u} \quad \text{or} \qquad \Delta \mathbf{F}_I^{\text{int}} = \sum_J \mathbf{K}_{IJ}^{\text{int}} \Delta \mathbf{u}_J \tag{22}$$

$$\Delta \mathbf{F}^{ext} = \mathbf{K}^{ext} \Delta \mathbf{u} \quad \text{or} \qquad \Delta \mathbf{F}_I^{ext} = \sum_J \mathbf{K}_{IJ}^{ext} \Delta \mathbf{u}_J \tag{23}$$

Where $\mathbf{K}^{\text{int}}$ and $\mathbf{K}^{ext}$ are the tangent stiffness matrices given by

$$\mathbf{K}_{IJ}^{\text{int}} = \frac{\partial \mathbf{F}_I^{\text{int}}}{\partial \mathbf{u}_J} = \frac{\partial^2 W^{\text{int}}}{\partial \mathbf{u}_I \partial \mathbf{u}_J}, \quad \mathbf{K}_{IJ}^{ext} = \frac{\partial \mathbf{F}_I^{ext}}{\partial \mathbf{u}_J} = \frac{\partial^2 W^{ext}}{\partial \mathbf{u}_I \partial \mathbf{u}_J} \tag{24}$$

Therefore, Newton equations can be obtained by linearization of Eq. (21) as

$$\left(\mathbf{K}^{\text{int}} - \mathbf{K}^{ext} \right) \Delta \mathbf{u} = -\mathbf{r} \tag{25}$$

2.4. *Nodal integration*
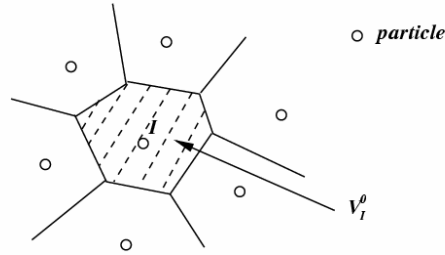
Fig. 1. Volume associated with particle I for nodal integration scheme

The integrals of Eq. (18) and Eq. (19) can be evaluated by numerical quadrature. Beissel and Belytschko [Beissel and Belytschko 1996] have proposed nodal integration scheme for the element-free Galerkin method [Belytschko et al. 1994], where any integral is evaluated by summing the function at particles, i.e.,

$$\int_{\Omega_0} F(\mathbf{X}) d\Omega = \sum_I F(\mathbf{X}_I) V_I^0 \tag{26}$$

where V_I^0 is the volume associated with particle I. Figure 1 shows that the volume can be calculated through the triangulation and Voronoi diagram. The internal nodal forces Eq. (19) can then be computed by

$$F_{iI}^{int} = \sum_I V_I^0 \frac{\partial w_I(\mathbf{X_I})}{\partial X_j} P_{ji}(\mathbf{X}_I) \tag{27}$$

This approach was found to be unstable by Beissel and Belytschko [Beissel and Belytschko 1996] in some cases, and it was verified by Belytschko and Xiao [Belytschko and Xiao 2002; Xiao and Belytschko 2005]. A stress point integration scheme was proposed [Dyka et al. 1997] to stabilize the nodal integration by adding some slave particles [Belytschko and Xiao 2002; Xiao and Belytschko 2004b]. However, we still use the nodal integration in this paper because it is simple and easy to implement. The stress point integration scheme will be added in further research investigation.

3. Implementation of the quasicontinuum method

3.1. *Molecular mechanics potential and discrete equations*

The general form for the molecular mechanics potential function can be expressed as the sum of the energies due to any force fields, such as the pair-wise interaction of the atoms, three-body potentials or others. It can be written as

$$W^M(\mathbf{x}_I) = \sum_I W_1(\mathbf{x}_I) + \sum_{I,J>I} W_2(\mathbf{x}_I, \mathbf{x}_J) + \sum_{I,J>I,K>J} W_3(\mathbf{x}_I, \mathbf{x}_J, \mathbf{x}_K) + \cdots \qquad (28)$$

Here, we assume that the total potential contains only the external energy and a pair-wise interatomic potential. The external energy is due only to a constant external force, $\mathbf{f}_I^{ext}$, such as electromagnetic forces. The pair-wise interatomic potential can be denoted by $w_{IJ} = w_M(\mathbf{x}_I, \mathbf{x}_J)$, so the total potential is

$$W^M = -W_M^{ext} + W_{IJ} = -\sum_I \mathbf{f}_I^{ext}\mathbf{d}_I + \sum_{I,J>I} w_M(\mathbf{x}_I, \mathbf{x}_J) \qquad (29)$$

where m_I is the mass of atom I, $\mathbf{x}_I$ is the current position of atom I and $\mathbf{x}_I = \mathbf{X}_I + \mathbf{d}_I$ ($\mathbf{X}_I$ is the original position of atom I and $\mathbf{d}_I$ is its displacement). Note that we use superscript/subscript "M" to denote the variable for a molecular system. A pair-wise interatomic potential can occur from bond stretching. Either the Lagrangian or the Hamiltonian mechanics can be used to derive the equations of motion at a molecular level.

In an isolated system of atoms or molecules, the total energy, the sum of the kinetic and potential energies of the molecules, is constant in time and identified as the Hamiltonian H^M, which is given by

$$H^M\left(\mathbf{x}_I(t), \mathbf{p}_I^M(t)\right) = \sum_I \frac{1}{2m_I}\mathbf{p}_I^M \cdot \mathbf{p}_I^M + W^M(\mathbf{x}_I(t)) = constant \qquad (30)$$

where m_I is the mass of atom I; $\mathbf{p}_I^M$ is the conjugate momentum and defined by

$$\mathbf{p}_I^M = m_I\dot{\mathbf{x}}_I = m_I\dot{\mathbf{d}}_I \qquad (31)$$

The well known Hamiltonian canonical equations of motion are

$$\dot{\mathbf{p}}_I^M = -\frac{\partial H}{\partial \mathbf{x}_I} = -\frac{\partial W^M}{\partial \mathbf{x}_I}, \quad \dot{\mathbf{x}}_I = \dot{\mathbf{d}}_I = \frac{\partial H}{\partial \mathbf{p}_I^M} = \frac{\mathbf{p}_I^M}{m_I} \qquad (32)$$

Eq. (32) can be combined to yield

$$m_I \ddot{\mathbf{d}}_I = -\frac{\partial W^M}{\partial \mathbf{x}_I} = \frac{\partial W_M^{ext}}{\partial \mathbf{d}_I} - \frac{\partial W_{IJ}}{\partial \mathbf{d}_I} = \mathbf{f}_I^{ext} - \mathbf{f}_I^{int} \qquad (33)$$

where $\mathbf{f}_I^{int} = \partial W_{IJ} / \partial \mathbf{d}_I$. Eq. (33) is a typical form for equations of motion solved in molecular dynamics. When one compares Eq. (33) with Eq. (17), it can be observed that the equations of motion are similar at the molecular level and the continuum level. For molecular mechanics, the equilibrium state of the molecular system can be obtained by setting the first derivatives of the potential, with respect to atomic displacements, to equal zero. The derived Newton equations are similar to Eq. (25). However, conjugate gradient methods are mostly used so that one can avoid calculating the second derivatives of the potential function.

3.2. *Quasicontinuum method*
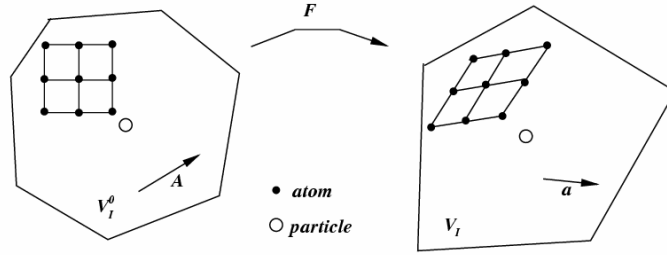
Fig. 2. Cauchy-Born rule for meshfree particle methods

In the quasicontinuum method, the intrinsic properties of material are sought at the atomic level and embedded in the continuum model according to a so-called Cauchy-Born rule [Tadmor et al. 1996; 2000]. The Cauchy-Born rule states that the deformation is locally homogeneous. In this paper, we assume that all the molecular structures in a single volume have the same deformation as the particle which the volume is associated with. As shown in Figure 2, an undeformed lattice vector $\mathbf{A}$ in V_I^0 is mapped into $\mathbf{a}$ in V_I by the deformation gradient $\mathbf{F}$ via $\mathbf{a} = \mathbf{FA}$. The molecular structures in V_I^0 are identically deformed according to the assumption of the Cauchy-Born rule. In the continuum model, with meshfree particle methods, the potential energy depends on the elongations and angle changes of the atomic bonds that underlie the volumes of particles. The total potential of the continuum model is defined by

$$W^C = \int_{\Omega_0} w_C d\Omega \qquad (34)$$

where w_C is the potential energy per unit volume of the continuum. Note that we use superscript/subscript "C" for variables in the continuum model to distinguish from the ones in the molecular model. The first Piola-Kirchhoff stress can be obtained from the potential density of the continuum by

$$\mathbf{P} = \frac{\partial w_C(\mathbf{F})}{\partial \mathbf{F}} \qquad (35)$$

The above serves as the constitutive equation for a continuum based on atomistic potentials. Therefore, the quasicontinuum approach is that the constitutive equation is constructed via the Cauchy-Born rule. If long distance interatomic interactions, such as nonbonded interaction, are considered, the van der Waals energy must be included in the molecular mechanics potential. Further research is needed to derive the continuum strain energy from the atomic-level potential and to modify the Cauchy-Born rule. Since the effects of long distance interatomic interactions on nanoscale mechanical behaviors of crystalline solids are not as significant as those of short distance interatomic interactions, we only consider short distance interatomic interactions in this paper.

With respect to the deformation gradients, the first tangential stiffness matrix can be obtained from the second derivatives of the potential density. It is

$$\mathbf{C} = \frac{\partial^2 w_C(\mathbf{F})}{\partial \mathbf{F}^2} \tag{36}$$

With the implementation of quasicontinuum method, the calculation of internal nodal forces, Eq. (19) can be written as

$$F_{iI}^{int} = \int_{\Omega_0} \frac{\partial w_I(\mathbf{X})}{\partial X_j} \frac{\partial w_C(\mathbf{F})}{\partial F_{ji}} d\Omega_0 \tag{37}$$

However, the classical Cauchy-Born rule has some difficulties for many important situations, such as in single-layer curved crystalline sheets. Arroyo and Belytschko [Arroyo and Belytschko 2002; 2003] developed an extension of the Cauchy-Born rule - the exponential Cauchy-Born rule. The objective of this extension is to account for the fact that the deformation gradient maps the tangent space of the undeformed surface to the tangent space of the deformed surface.

It should be noted here that the classical Cauchy-Born rule are valid for isolated systems as microcanonical ensembles. For other ensembles, modifications of the quasicontinuum method (Cauchy-Born rule) are needed. For example, the recently developed finite temperature quasicontinuum method [Diestler et al. 2004] must be used for canonical ensembles with thermostats.

3.3. Continuum model for a molecule chain
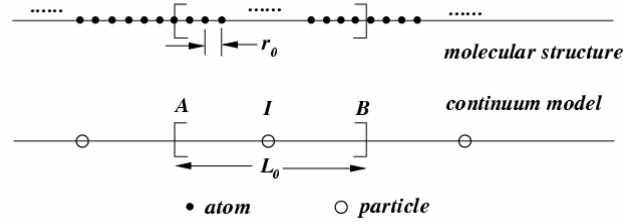
Fig. 3. A continuum model for a molecular chain with the meshfree particle method

A line of atoms as well as its continuum model in the reference (initial) configuration is considered here as shown in Figure 3. The equilibrium bond length between neighboring atoms is r_0, and the length of the region AB associated with the particle I is

L_0. We assume that only the nearest two atoms are attractive and repulsive with each other. Therefore, the molecular potential can be written as follows without considerations of external forces:

$$W = \sum_{i=2}^{N} w_M (x_i - x_{i-1}) = \sum_{i=1}^{N-1} w_M (r_i) \tag{38}$$

where N is the total number of atoms; $r_i = x_{i+1} - x_i$ is the current bond length. If we use F_I to denote the deformation gradient at particle I, all the deformed bonds in region AB will have the same length, $r = F_I r_0$, according to the assumption of the Cauchy-Born rule. One can write the potential density of the volume associated with particle I based on the atomic level potential as

$$w_C(F_I) = \frac{W^C(F_I)}{L_0} = \frac{\dfrac{L_0}{r_0} w_M(r)}{L_0} = \frac{w_M(r)}{r_0} = \frac{w_M(F_I r_0)}{r_0} \tag{39}$$

Then, the first Piola-Kirchhoff stress can be calculated as

$$P(X_I) = \frac{\partial w_C(F_I)}{\partial F_I} = \frac{1}{r_0} \frac{\partial w_M(F_I r_0)}{\partial F_I} \tag{40}$$

As an instance, we use the Lennard-Jones (LJ) 6-12 potential to approach the interaction between the nearest atoms. The LJ 6-12 potential function is written as

$$w_M = 4\varepsilon \left[\left(\frac{\sigma}{r} \right)^{12} - \left(\frac{\sigma}{r} \right)^{6} \right] \tag{41}$$

where ε and σ are constants chosen to fit material properties and r is the distance between two atoms. ε is the depth of the potential energy well. σ is the value of r where the potential becomes zero and $\sigma = 2^{-1/6} r_0$. The potential energy density at particle I can be written as follows from Eq. (39):

$$w_C(F_I) = \frac{w_M(F_I r_0)}{r_0} = \frac{4\varepsilon}{r_0} \left[\left(\frac{\sigma}{r_0} \right)^{12} F_I^{-12} - \left(\frac{\sigma}{r_0} \right)^{6} F_I^{-6} \right] \tag{42}$$

Therefore, the first Piola-Kirchhoff stress at particle I can be obtained as

$$P(X_I) = \frac{\partial w_C}{\partial F_I} = \frac{4\varepsilon}{r_0} \left[\frac{6\sigma^6}{r_0^6 F_I^7} - \frac{12\sigma^{12}}{r_0^{12} F_I^{13}} \right] \tag{43}$$

3.4. *Continuum model for a molecular structure with triangular lattices*

Here, we consider a 2D molecular structure with triangular lattices as shown in Figure 4. This molecular structure was used by Gao [Gao 1996] to study the local limiting speed in dynamic fractures. A pair potential function of $U(l)$ is used here to describe the nearest-neighbor interatomic interaction. l denotes the bond length and $l = l_0$ when the bond is not stretched i.e. when the bond is at the equilibrium state. Figure 4 also shows that a rectangle cell is set as a unit cell to calculate the continuum properties of the molecular structure.
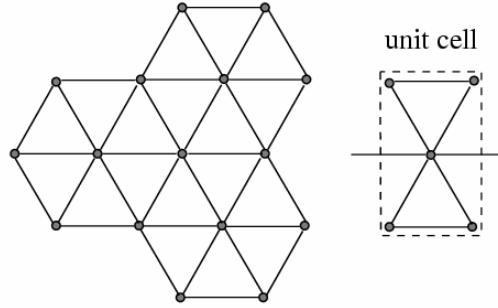
Fig. 4 A molecular structure with triangular lattices

We assume that the volume associated with a particle contains a large number of such unit cells. If a unit cell is under the deformation with the deformation gradient $\mathbf{F}$, then there are three types of deformed bonds as shown in Figure 5. Therefore, the strain energy per undeformed unit area (strain energy density) in such a unit cell is

$$w_C = \frac{2}{\sqrt{3}l_0}\left[U(l_1)+U(l_2)+U(l_3)\right] \tag{44}$$

where l_1, l_2, l_3 can be described by deformation gradient $\mathbf{F}$ based on the geometric relations, one can find that

$$
\begin{aligned}
l_1 &= l_0\sqrt{F_{11}^2 + F_{21}^2} \\
l_2 &= l_0\sqrt{(\tfrac{1}{2}F_{11}-\tfrac{\sqrt{3}}{2}F_{12})^2 + (\tfrac{1}{2}F_{21}-\tfrac{\sqrt{3}}{2}F_{22})^2} \\
l_3 &= l_0\sqrt{(\tfrac{1}{2}F_{11}+\tfrac{\sqrt{3}}{2}F_{12})^2 + (\tfrac{1}{2}F_{21}+\tfrac{\sqrt{3}}{2}F_{22})^2}
\end{aligned}
\tag{45}
$$
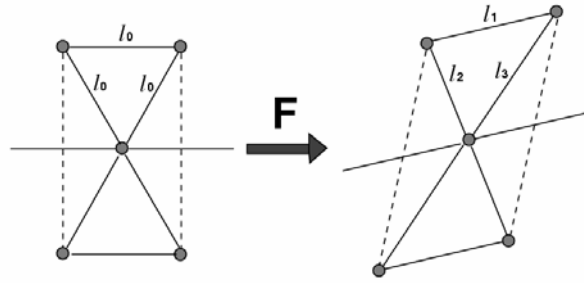
Fig. 5 Deformation of a unit cell

The first Piola-Kirchhoff stress $\mathbf{P}$ is the first derivative of strain energy density with respect to the deformation gradient, and one can have

$$\mathbf{P} = \frac{2}{\sqrt{3}l_0}\left[\frac{\partial U(l_1)}{\partial \mathbf{F}} + \frac{\partial U(l2)}{\partial \mathbf{F}} + \frac{\partial U(l_3)}{\partial \mathbf{F}}\right]$$

$$= \frac{2}{\sqrt{3}l_0}\left[\frac{\partial U(l_1)}{\partial l_1}\frac{\partial l_1}{\partial \mathbf{F}} + \frac{\partial U(l_2)}{\partial l_2}\frac{\partial l_2}{\partial \mathbf{F}} + \frac{\partial U(l_3)}{\partial l_3}\frac{\partial l_3}{\partial \mathbf{F}}\right]$$

(46)

and the components of the stress are

$$P_{11} = \frac{2}{\sqrt{3}l_0}\left[\frac{\partial U(l_1)}{\partial l_1}\frac{F_{11}}{l_1} + \frac{\partial U(l_2)}{\partial l_2}\frac{1}{2l_2}\left(\frac{1}{2}F_{11} - \frac{\sqrt{3}}{2}F_{12}\right) + \frac{\partial U(l_3)}{\partial l_3}\frac{1}{2l_3}\left(\frac{1}{2}F_{11} + \frac{\sqrt{3}}{2}F_{12}\right)\right]$$

$$P_{12} = \frac{2}{\sqrt{3}l_0}\left[-\frac{\partial U(l_2)}{\partial l_2}\frac{\sqrt{3}}{2l_2}\left(\frac{1}{2}F_{11} - \frac{\sqrt{3}}{2}F_{12}\right) + \frac{\sqrt{3}}{2l_3}\frac{\partial U(l_3)}{\partial l_3}\left(\frac{1}{2}F_{11} + \frac{\sqrt{3}}{2}F_{12}\right)\right]$$

$$P_{21} = \frac{2}{\sqrt{3}l_0}\left[\frac{\partial U(l_1)}{\partial l_1}\frac{F_{21}}{l_1} + \frac{\partial U(l_2)}{\partial l_2}\frac{1}{2l_2}\left(\frac{1}{2}F_{21} - \frac{\sqrt{3}}{2}F_{22}\right) + \frac{1}{2l_3}\frac{\partial U(l_3)}{\partial l_3}\left(\frac{1}{2}F_{21} + \frac{\sqrt{3}}{2}F_{22}\right)\right]$$

$$P_{22} = \frac{2}{\sqrt{3}l_0}\left[-\frac{\partial U(l_2)}{\partial l_2}\frac{\sqrt{3}}{2l_2}\left(\frac{1}{2}F_{21} - \frac{\sqrt{3}}{2}F_{22}\right) + \frac{\sqrt{3}}{2l_3}\frac{\partial U(l_3)}{\partial l_3}\left(\frac{1}{2}F_{21} + \frac{\sqrt{3}}{2}F_{22}\right)\right]$$

Correspondingly, the first tangential stiffness matrix can be written as

$$\mathbf{C} = \frac{\partial^2 w_C}{\partial \mathbf{F} \partial \mathbf{F}} = \frac{\partial \mathbf{P}}{\partial \mathbf{F}}$$

(47)

4. Examples

4.1. *Wave propagation in a molecular chain*
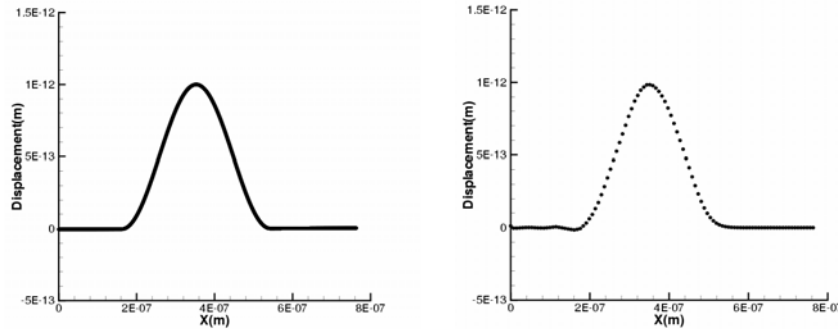
(a) molecular dynamics   (b) meshfree particle method

Fig. 6.   Wave propagation in a molecule chain

Wave propagation along a one-dimensional molecule chain is studied by using molecular dynamics and the meshfree particle method with quasicontinuum implementation separately. The molecule chain contains 2,001 atoms. 101 particles are

used in the meshfree particle simulation. The L-J (6-12) potential function is used to approach the interaction between the nearest atoms. The constants are chosen as: $\sigma = 3.4e^{-10}m$ and $\varepsilon = 1.65e^{-21}J$. The mass of each atom is set to be $3.8 \times 10^{-10}kg$. In the meshfree particle method, the first Piola-Kirchhoff stress can be obtained from Eq. (43). Figure 6 shows the comparison of the calculated wave configurations at $t = 0.02ns$, from the molecular dynamics simulation and the meshfree particle method, when an initial cosine shaped wave is given. We can see that they are in accord.

4.2. Bending of a nanobeam

In this example, we consider the bending of a nano cantilever beam. The beam contains 5,140 atoms as shown in Figure 7 where $L = 270nm$ and $H = 15.6nm$. One end of the beam is fixed. A quadratic potential function is used to approximate the interaction between nearest atoms,

$$U(l) = \frac{1}{2}k(l - l_0)^2 \tag{48}$$

where $k = 10000N/m$ and $l_0 = 1nm$.
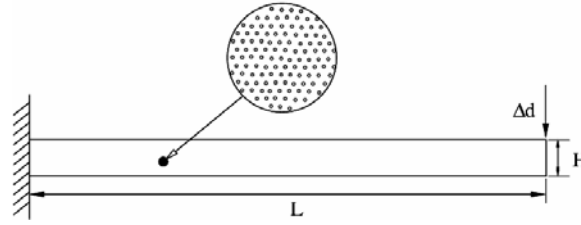
Fig. 7. A nano cantilever beam

We use the meshfree particle method to simulate the bending of this nanobeam, which is under the load of a prescribed displacement as shown in Figure 7. There are 250 particles used in the simulation. In the meshfree particle method, the first Piola-Kirchhoff stress and tangential stiffness matrix can be calculated when substituting Eq. (48) into Eq. (46) and Eq. (47). During the simulation, the prescribed displacement will be increased by $\Delta d = 3.6nm$ per calculation step. After 50 steps, the nanobeam will be bent as the final configuration shown in Figure 8(a).

We also show the molecular mechanics calculation result for comparison. One can see that the outcome in Figure 8 (b) supports the meshfree particle method result. When different numbers of particles are used in the meshfree particle method simulations, Figure 9 shows the evolution of the calculated nanobeam potential compared with the molecular mechanics result. We can see that the meshfree particle method with 250 particles gives a consistent response with the molecular mechanics calculation. If 1,000 or more particles are used in the simulations, the evolution of the nanobeam potential is almost identical to the one from the molecular mechanics calculation.
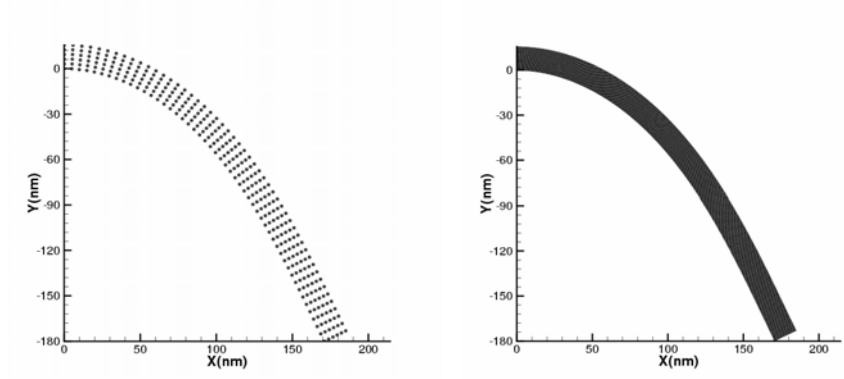
(a) meshfree particle method   (b) molecular mechanics
Fig 8 Deformed configurations of the nanobeam
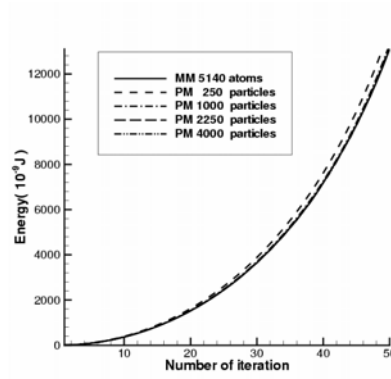
Fig 9 Comparison of evolutions of the nanobeam potential

We study the convergence by using the l_2 error in displacement for the nanoscale meshfree particle method. The error in displacement is defined as

$$Error = \frac{\left\| \mathbf{u}^{MM} - \mathbf{u}^{PM} \right\|_2}{\left\| \mathbf{u}^{MM} \right\|_2} \tag{49}$$

where $\mathbf{u}^{MM}$ and $\mathbf{u}^{PM}$ are the atomic displacements from the molecular mechanics calculation and the meshfree particle method, respectively. Note, here, that one can calculate the atomic displacements from the particle displacements in the meshfree particle method based on the meshfree particle approximation.
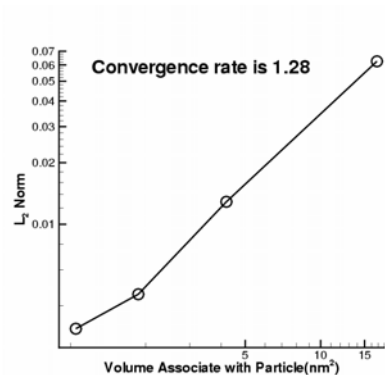
Fig 10 Convergence of the nanoscale meshfree particle method

4.3. *Vibration of a nanobeam*

The vibration of a nano cantilever beam is studied in this example. The nanobeam is similar to what we study in the previous examples, but with $L = 200nm$ and $H = 34.6nm$. There are 8,221 atoms in this nanobeam. One end of the beam is fixed. We use the LJ (6-12) potential function to approximate the interaction between nearest atoms. The constants are chosen as follows: $\sigma = 1.833nm$ and $\varepsilon = 8.25e^{-9}J$. The mass of each atom is $5.0e^{-17}kg$. In this example, the nanobeam is bent first with the loading of a prescribed displacement at the upper right corner. This step can be achieved similarly with the technique we used in the previous example. Then, if the nanobeam is released, it will vibrate up and down. Different numbers of particles are used in the simulations. The calculated oscillatory amplitude and frequency of the middle point on the right boundary are compared with the molecular dynamics simulation results as shown in Table 1, as well as computer time, when two vibration circles are finished. We can see that molecular dynamics simulations are obviously computationally intensive and the continuum mechanics (meshfree particle methods here) can save a great amount of computing time. Furthermore, the meshfree particle methods can give very accurate values of the oscillatory amplitudes compared with molecular dynamics, but not the frequencies although they are still compared well. We think that this result is due to the vibration of atoms around their equilibrium positions. Such molecular-level phenomena results in one of the macroscopic properties, temperature. How to couple the temperature effects within the continuum mechanics is one of the issues that the hierarchical multiscale methods need to solve.

Table 1. Amplitudes and frequencies of nanobeam vibration.

	Amplitude (nm)	Frequency (1/ns)	CPU time (s)
Molecular dynamics (8,221 atoms)	3.90	2.067	425.25
Meshfree particle method (2,000 Particles)	3.91	2.159	52.46
Meshfree particle method (320 Particles)	3.93	2.272	11.53
Meshfree particle method (80 Particles)	3.94	2.324	2.31

4.4. *A plate with a central crack*

Meshfree particle methods have advantages to treat fracture problems. In this example, we use the meshfree particle method to study the stress concentration of a nanoplate containing an initial central crack. The crack is initialized by taking a number of bonds out. The meshfree particle model with 400 particles is shown in Figure 11. The dimensions are: $L = 270nm$ and $M = 280nm$, and the crack length is $135nm$. This nanoplate contains 86,915 atoms with the triangular molecular structure. The LJ (6-12) potential function is used in this example as the previous one. We use a visibility criterion [Belytschko et al. 1994] in the meshfree particle model to construct the kernel functions for the particles near the crack or around the crack tip, as illustrated in Figure 12. When we plan to search the neighbor particles for particle I , we take particle K into account, but not particle J , since one cannot see particle J from particle I , due to the block of the crack. It should be noted here that the visibility criterion can result in discontinuities in kernel functions of particles near crack tips. Other techniques, the diffraction method and the transparency method [Organ et al. 1996], can provide continuous and smooth approximations near nonconvex boundaries. For simplification, we use the visibility criterion in this paper.
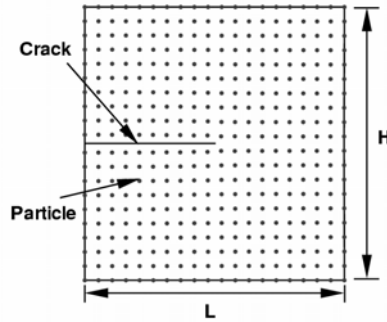
Fig 11. A nanoplate with a central crack modeled by the meshfree particle method
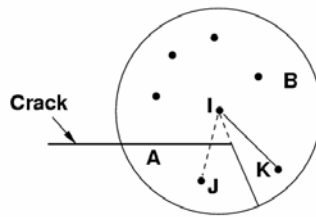
Fig. 12. Visibility criterion in the meshfree particle method

We plan to observe the stress concentration around the crack tip. The constitutive relationship can be achieved through the Cauchy-Born rule as before. For the purpose of comparison, we also perform molecular mechanics calculations to obtain the contour of

stress distribution. At the atomic level, the Cauchy stress [Zhou 2003] can be calculated as the following formula:

$$\boldsymbol{\sigma} = \frac{1}{2\Omega} \sum_i^N \sum_{j,j\neq i}^N \mathbf{r}_{ij} \otimes \mathbf{f}_{ij} \qquad \text{or} \qquad \sigma_{\alpha\beta} = \frac{1}{2\Omega} \sum_i^N \sum_{j,j\neq i}^N r_{ij}^\alpha f_{ij}^\beta \qquad (50)$$

where $\boldsymbol{\sigma}$ is the Cauchy stress, m_i is the mass of atom i, $\dot{\mathbf{r}}_i$ is the time derivative of atomic position $\mathbf{r}_i$, $\mathbf{r}_{ij} = \mathbf{r}_i - \mathbf{r}_j$ is the spatial vector between atoms i and j, and $\otimes$ denotes the tensor product of two vectors. The parameter N is the total number of atoms in the domain Ω. The interatomic force $\mathbf{f}_{ij}$ applied on atom i by atom j is:

$$\mathbf{f}_{ij} = -\frac{\partial \Phi_{ij}}{\partial r_{ij}} \frac{\mathbf{r}_{ij}}{r_{ij}} \qquad (51)$$

where Φ_{ij} is the interatomic potential between atoms i and j. The sign is adopted here for force, which is positive for repulsion and negative for attraction.

Figure 13 shows the comparison of the stress (σ_{yy}) contour from the molecular mechanics calculation and the meshfree particle simulation. In the molecular mechanics calculation, the whole domain is divided into a number of subdomains, for each of which the Cauchy stress can be computed via Eq. (50). We can see that the result of meshfree particle method is in accord with that of the molecular mechanics calculation.

(a) molecular mechanics   (b) meshfree particle method
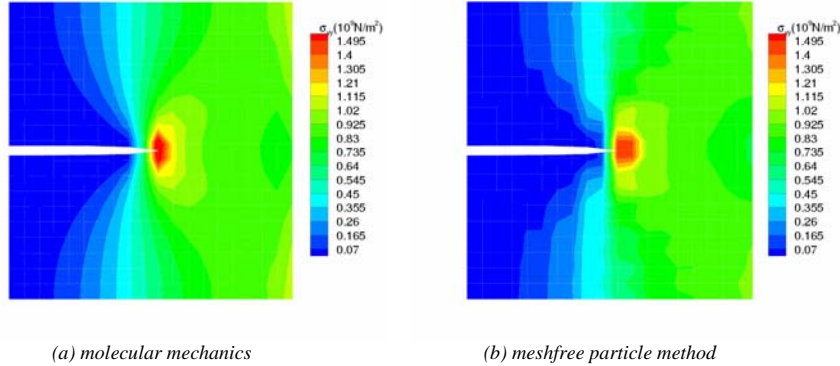
Fig 13. Comparison of stress concentration

5. Conclusions

In this paper, we implemented a quasicontinuum technique (Cauchy-Born rule) into the meshfree particle methods. Therefore, numerical simulations in nanotechnology can be beneficial from the advantages of the meshfree particle methods. This progress makes it possible to treat extremely large deformation problems and the problems involving discontinuities, such as fractures, at nanoscale. The developed nanoscale meshfree particle method is one of the hierarchical multiscale methods and has been shown to save a great amount of computer time. The static examples show that this method can give accurate results when compared with the molecular mechanics calculation outcomes.

However, we observed that the dynamic solutions from this nanoscale meshfree particle method are not as reliable as the static solutions when they are compared with the molecular dynamics results. We think that this is due to the temperature issue since no temperature effects are considered in our nanoscale meshfree particle method. This issue will be discussed in our further publications.

Acknowledgments

References

Abraham, F., Broughton, J., Bernstein, N. and Kaxiras, E. (1998). Spanning the continuum to quantum length scales in a dynamic simulation of brittle fracture. *Europhys. Lett.*, **44**: 783-787.

Arroyo, M. and Belytschko, T. (2002). An atomistic-based finite deformation membrane for single layer crystalline films. *J. Mech. Phys. Solids,* **50:** 1941-1977.

Arroyo, M. and Belytschko, T. (2003). A finite deformation membrane based on inter-atomic potentials for the transverse mechanics of nanotubes. *Mech. Mater.*, **35:**193-215

Beissel, S. and Belytschko, T. (1996). Nodal integration of the element-free Galerkin method. *Comp. Meth. Appl. Mech. Engng.,* **139:** 49-74

Belytschko, T., Lu, Y. Y. and Gu, L. (1994). Element-free Galerkin methods, *Int. J. Numer. Meth. Engng.,* **37:** 229-256.

Belytschko, T., Krongauz, Y., Dolbow, J. and Gerlach, C. (1998). On the completeness of meshfree particle methods. *Int. J. Numer. Mech. Engng.,* **43:** 785-819.

Belytschko, T., Guo, Y., Liu, W. K. and Xiao, S. P. (2000). A unified stability analysis of meshless particle methods, *Int. J. Numer. Meth. Engng.,* **48:**1359-1400

Belytschko, T., Liu, W. K. and Moran, B. (2001) *Nonlinear Finite Elements for Continua and Structures*, Wiley, New York.

Belytschko, T. and Xiao, S. P. (2002). Stability analysis of particle methods with corrected derivatives. *Comp. Math. Appl.,* **43:**329-350

Belytschko, T. and Xiao, S. P. (2003). Coupling methods for continuum model with molecular model, *Int. J. Mult. Comp. Engrg.,* **1:** 115-126.

Broughton, J., Abraham, F., Bernstein, N. and Kaxiras, E. (1999). Concurrent coupling of length scales: Methodology and application. *Phys. Rev. B,* **60:** 2391-2403.

Diestler, D. J. (2002). Coarse-grained descriptions of multiple scale processes in solid systems. *Phys. Rev. B,* **66:** 184104

Diestler, D. J., Wu, Z. B. and Zeng, X. C. (2004). An extension of the quasicontinuum treatment of multiscale solid systems to nonzero temperature. *J. Chem. Phys.,***121(19):** 9279-9282

Dyka, C. T., Randles, P. W. and Ingel, R. P. (1997). Stress points for tension instability in SPH. *Int. J. Numer. Meth. Engng.,* **40:** 2325-2341

Gao, H. (1996). A theory of local limiting speed in dynamic fracture. *J. Mech. Phys. Solids.* **44:** 1453-1474.

Mortensen, J. J., Schiøtz, J. and Jacobsen, K.W. (2002). The quasicontinuum method revisited. *Chall. Mole. Simul.,* ed. D. Mac Kernan, SIMU Newsletter **4**, 119.

Organ, D. J., Fleming, M. and Belytschko, T. (1996). Continuous meshless approximations for nonconvex bodies by diffraction and transparency. *Comput. Mech.,* **18:**225-235.

Rabczuk, T., Belytschko, T. and Xiao, S. P. (2004). Stable particle methods based on Lagrangian kernels. *Comp. Meth. Appl. Mech. Engng.,* **193:** 1035-1063.

Randles, P. and Libersky, L. (1996). Smoothed particle hydrodynamics: Some recent improvements and applications, *Comp. Meth. Appl. Mech. Engng.,* **139:**375-408

Rodney, D. and Phillips, R. (1999). Structure and strength of dislocation junctions: an atomic level analysis. *Phys. Rev. Lett.,* **82:** 1704-1707

Rudd, R. E. and Broughton, J. (1998). Coarse-grained molecular dynamics and the atomic limit of finite elements. *Phys. Rev. B,* **58:** R5893-R5896

Rudd, R. E. (2001). Concurrent multiscale simulation and coarse-grained molecular dynamics. *Abs. Pap. Amer. Chemical Soc.,* **221:** 208.

Smith, G. S., Tadmor, E. B., Bernstein, N. and Kaxiras, E. (2001). Multiscale simulations of silicon nanoindentation. *ACTA Mater.,* **49:** 4089-4101.

Tadmor, E. B., Ortiz, M. and Phillips, R. (1996). Quasicontinuum analysis of defects in solids. *Phil. Mag. A,* **73:** 1529-1563.

Tadmor, E. B., Phillips, R. and Ortiz, M. (2000). Hierarchical modeling in the mechanics of materials. *Int. J. Solids Strut.,* **37:** 379-389.

Wagner, G. J. and Liu, W. K. (2003). Coupling of atomic and continuum simulations using a bridging scale decomposition. *J. Comp. Phys.,* **190:** 249-274.

Wu, Z. B., Diestler, D. J., Feng, R. and Zeng, X. C. (2003). Coarse-graining description of solid systems at nonzero temperature. *J. Chem. Phys.,* **119**: 8013-8023.

Xiao, S. P. and Belytschko, T. (2004). A bridging domain method for coupling continua with molecular dynamics. *Comp. Meth. Appl. Mech. Engrg.,* **193:** 1645-1669.

Xiao, S. P. and Belytschko, T. (2005). Material stability analysis of particle methods. *Adv. Comp. Math.*, **23:** 171-190.

Zhou, M., (2003). A new look at the atomic level virial stress: on continuum-molecular system equivalence. *Proc. R. Soc. Lond. A,* **459:**2347-2392.